https://dx.doi.org/10.1016/j.jmapro.2020.10.069

Novel fluid line-jet polishing of rotational axisymmetric surfaces

C.J. Wang, C.F. Cheung*, L.T. Ho, Y.M. Loh

State Key Laboratory of Ultra-precision Machining Technology, Department of Industrial and Systems Engineering, The Hong Kong Polytechnic University, Hung Hom, Kowloon, Hong Kong, China

*Corresponding author: benny.cheung@polyu.edu.hk

Abstract

In this paper, a novel fluid line-jet polishing (FLJP) process was developed for the polishing of rotational axisymmetric surface (RAS). FLJP aims to enhance the polishing efficiency of fluid jet polishing without degrading the polished surface integrity, together with better material removal uniformity than linear-array multi-jet polishing (MJP). The fluid field was analyzed by comparing to the traditional fluid jet polishing (FJP) based on computational fluid dynamics (CFD) method so as to test the stability of the fluid line-jet. A series of polishing experiments were conducted to analyze the performance of the FLJP and compared to FJP and MJP in terms of material removal characteristics, the effect of the main factors, material removal uniformity and surface quality after polishing on cylindrical surfaces. The results indicate that FLJP has much higher material removal rate than FJP under the same polishing conditions together with good surface quality. Moreover, the material removal after FLJP is much more uniform than MJP. Hence, the result demonstrates that the FLJP process is effective for polishing of RAS.

Keywords

Fluid line-jet polishing; fluid jet polishing; rotational axisymmetric surface; roller surface; computational fluid dynamics; ultra-precision machining

1 Introduction

Rotational axisymmetric surface (RAS) here signifies a surface can be generated through the rotation of one line or curve along a central axis, which have been widely used in the industries, such as roller surfaces and precision molds [1,2], internal cylindrical surfaces used for gas and fluid flow applications in aerospace and automotive industries [3], etc. Polishing of these kinds of surface are usually conducted to obtain high quality surface with much better performance. Fluid jet polishing (FJP) [4,5], as one of the promising ultra-precision polishing process, has been successfully used in super-finishing of various kinds of freeform surfaces made of a variety of difficult-to-machine materials [6-8], including cylindrical optical mandrels [9]. Different from high pressure abrasive waterjet machining process [10-12], the water and abrasive are premixed thoroughly in the slurry tank, and pressurized at low pressure (normally smaller than 2.0 MPa) to impinge the target surface. In comparison to other polishing processes, its unique advantages include no temperature raise during polishing, no tool wear, more adaptive to various kinds of freeform surfaces, and wide material applicability.

The main drawback of FJP is the low material removal rate, and it can hardly be used for the polishing of medium-large size surfaces [13,14]. According to the literatures [5,15], the material removal rate can be increased by increasing the fluid pressure, abrasive size and slurry concentration. Nevertheless, high fluid pressure and large abrasive size would lead to poor surface finish, while high slurry concentration would not only make it difficult to control its stability, but also lead to the congestion of the slurry system. Messelink et al. [16] and Yu et al. [17] attempted to add pressurized gas into the fluid jet to enhance the polishing efficiency, but the polished surface has severe surface

defects and much poorer surface finish than traditional fluid jet polishing (FJP). Beaucamp et al. [13] innovatively adopted the ultrasonic cavitation phenomenon to assist FJP, which successfully boosted the material removal rate without degrading the surface integrity, and the enhancement of the removal rate is about 4 times of FJP under the same conditions. The authors [14,18,19] have developed the multi-jet polishing (MJP) method to improve the polishing efficiency of FJP recently, it can largely increase the material removal rate. The boosted efficiency is almost proportional to the number of orifices in the multi-jet nozzle. The MJP process can also maintain the surface integrity as well as FJP. However, the jet interference between fluid jets leads to the discontinuous tool influence function, which is not conducive for the uniform polishing of RAS [20].

To address this problem, a novel fluid line-jet polishing (FLJP) process is presented in this paper, which not only largely enhances the polishing efficiency of FJP without degrading the surface integrity, but also achieves better uniform material removal than linear distributed multi-jet polishing when polishing the RASs. The principle of FLJP is discussed in section 2. In section 3, the experiments are conducted and described in details to analyze its performance in four aspects, including material removal rate, material removal controllability, material removal uniformity, and polished surface integrity. Section 4 discusses the applications of FLJP depending on different polishing modes. The conclusions are made in section 5.

2 Working principle of fluid line-jet polishing (FLJP)

2.1 Fluid line-jet polishing system

Figure 1 shows the schematic diagram of the FLJP system, which mainly includes the mechanical movement system and slurry pressure control and circulation system. The orifice shape is long and

narrow rectangle with semicircles at the two sides as shown in Fig. 1. During polishing, the pressurized slurry is transported to the line-jet nozzle, and impinged out from the line shape orifice to generate a fluid line-jet. Abrasives in the slurry could be cerium oxide (CeO_2), aluminum oxide (Al_2O_3), silicon oxide (SiO_2), silicon carbide (SiC), etc., depending on the material of the target surfaces being polished. The fluid pressure is controlled in the range from2 bar to20 bar. As compared to FJP, FLJP owns much larger contact area between the fluid jet and target surface under the same polishing conditions, which attributes to larger material removal rate. The ratio of the section area of the fluid jet between FLJP and FJP η can be expressed as:

$$\eta = \frac{LD + \pi(D/2)^2}{\pi(D/2)^2} = \frac{4L}{\pi D} + 1 \tag{1}$$

where L is the length of the line orifice, and D is the diameter of the FJP orifice, which is also the width of the line orifice as shown in Fig. 1. η is directly proportional to the ratio between L and D as can be seen from Eq. (1).

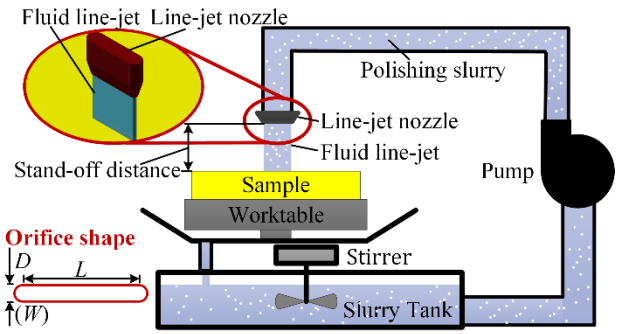

Fig. 1 Schematic diagram of the fluid line-jet polishing system.

2.2 Fluid flow field analysis in fluid line-jet polishing

The stability of the fluid jet is crucial to obtain high surface quality. Hence, the analysis of the fluid

field in FLJP was conducted here based on Computational Fluid Dynamics (CFD) method. The simulation was implemented in ANSYS FLUENT 17.2 software package. The Volume of Fluid (VOF) model was adopted in the multiphase solution based on the assumption that the fluid flow is incompressible, and operates with constant density and temperature conditions. The incompressible form of the Navier-Stokes equation can be used in such case to describe the fluid velocity field [6]:

$$\rho(\frac{\partial v}{\partial t} + v \cdot \nabla v) = -\nabla p + \mu \nabla^2 v + f \tag{2}$$

where ρ is the fluid density, v is the fluid velocity, p is the fluid pressure, μ is the fluid viscosity, and f is the external forces acted on the fluid. For turbulence modeling, the Shear Stress Transport (SST) based on a blending of the k-ω and k-ε turbulence models is used to express the turbulent fluid flow in the inner region of the boundary layer as well as in the outer art of the boundary layer for a wide range of the Reynolds number. And the detailed modeling method can refer to our previous publication [21]. Fluid field of the FLJP adopting two line orifices with different lengths was compared to FJP. Figure 2 shows the simplified mesh model designed for the CFD simulation of these three situations. The diameter of the normal orifice is 0.5 mm. The width of two line-orifices is also 0.5 mm, while the length of them are 3 mm and 6 mm, respectively. The fluid pressure is 8 bar, and the stand-off distance (SOD) is 5 mm. The SOD is the distance between the orifice and the target surface as shown in Fig. 1.

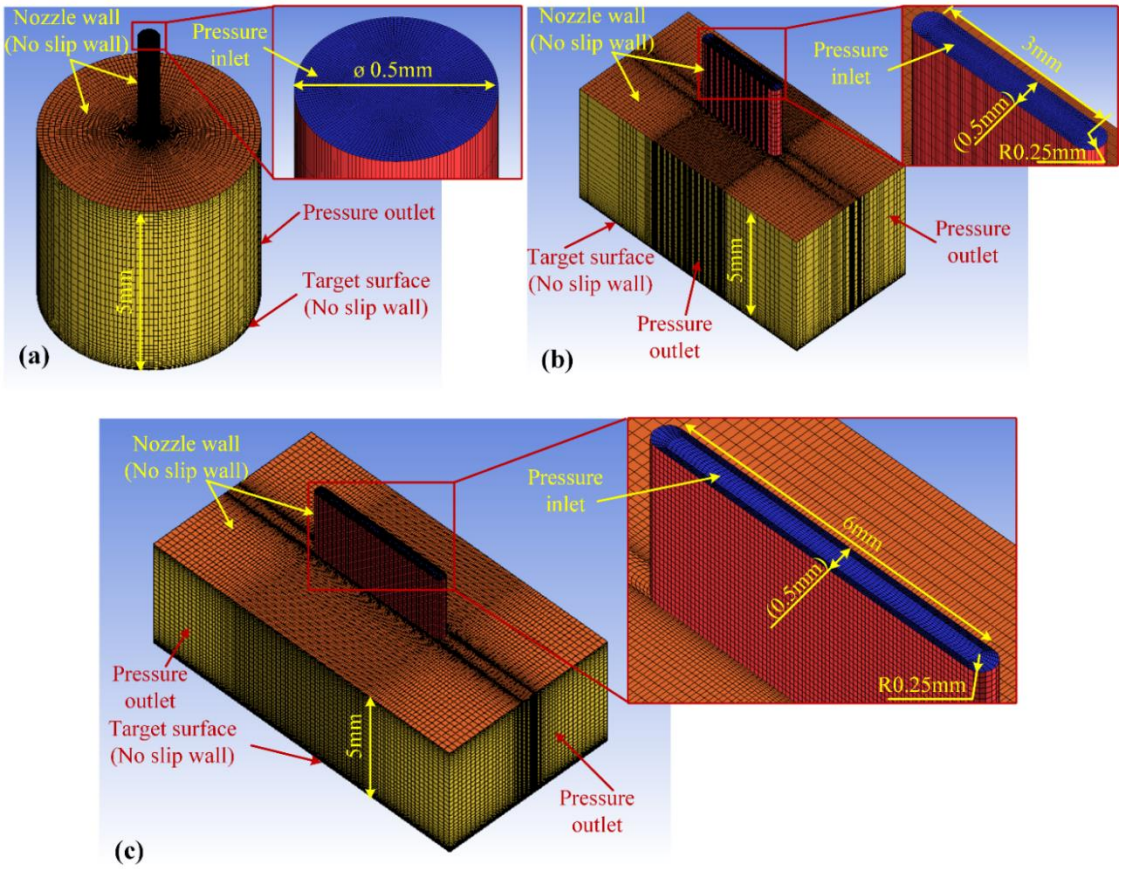

Fig. 2 Mesh models for computational fluid dynamic analysis of three kinds of nozzles: (a) fluid jet polishing (D=0.5mm), (b) fluid line-jet polishing (L=3mm), (c) fluid line-jet polishing (L=6mm).

Figure 3 shows the simulation results of their fluid field. The velocity distribution has been shown in Fig. 3(a). To compare them quantitatively, sectional profile along the line with a distance of 3 mm to the orifice has also been extracted and presented in Fig. 3(c). The velocity distribution trend in FLJP is similar to FJP, which is the largest at the center region of the fluid jet and decreases to the edge. However, it is interesting to note that FLJP has much wider uniform velocity region inside the fluid jet as compared to FJP as shown in Fig. 3(c). It is beneficial to obtain higher material removal rate and

uniform material removal.

Aiming to evaluate the fluid jet stability of FLJP, the turbulence intensity was adopted as the evaluation indicator. The turbulence intensity I [22], which is often referred to as turbulence level, is defined as the ratio of the root-mean-square of the velocity fluctuations u', to the mean flow velocity U, as shown as follows:

$$I = \frac{u'}{U} \tag{3}$$

$$u' = \sqrt{\frac{1}{3}(u_x'^2 + u_y'^2 + u_z'^2)} \tag{4}$$

$$U = \sqrt{U_x^2 + U_y^2 + U_z^2} \tag{5}$$

where u_x', u_y', u_z' are three components of u', and U_x, U_y, U_z are three components of U. Small turbulence intensity signifies low fluid turbulence. Figure 3(b) shows the simulation results of their turbulence intensity distribution on the section view. Their sectional profiles were also extracted and demonstrated in Fig. 3(d). The maximum value of the turbulence intensity between FJP and FLJP as shown in Fig. 3(d), which indicates that the line-jet in FLJP is as stable as in FJP. Moreover, the turbulence intensity of most part of the fluid jet in FLJP is at small scale as compared to FJP. Hence, it suggests that the stability of the fluid jet is not degraded in FLJP as compared to FJP.

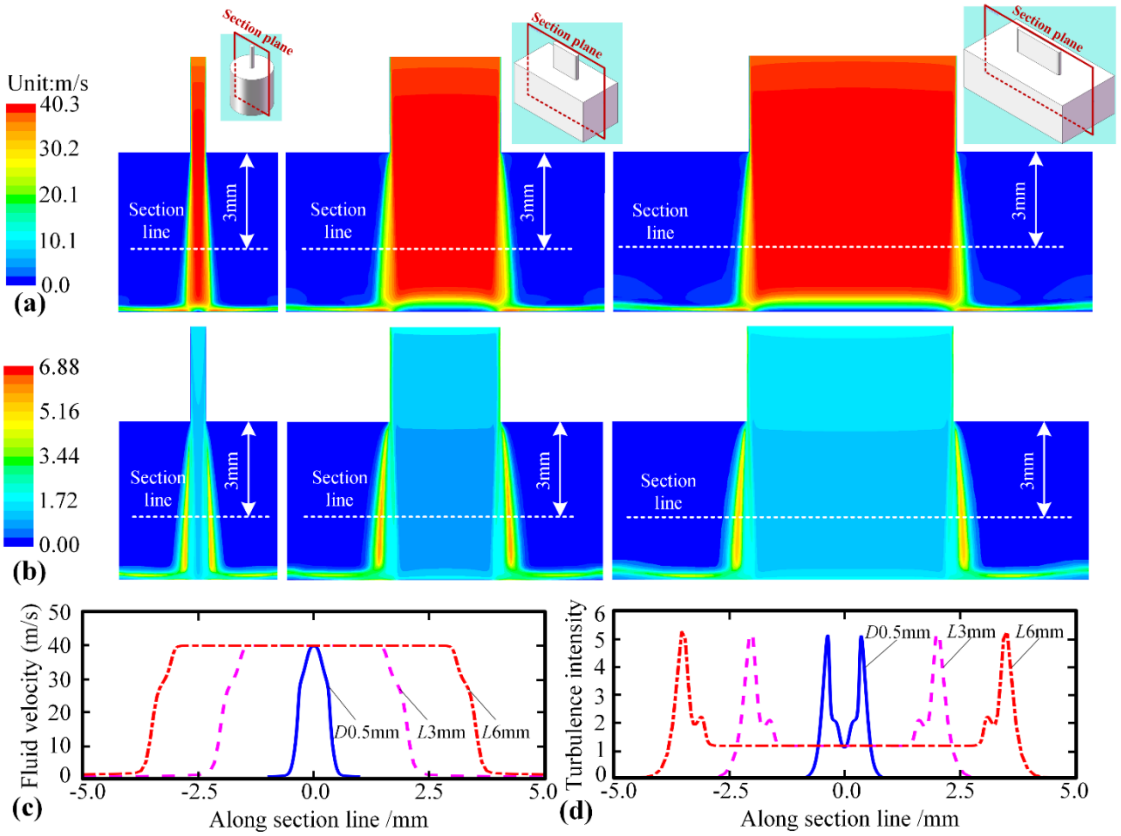

Fig. 3 Fluid field comparison between normal fluid jet polishing (D = 0.5 mm) and two kinds of fluid line-jet polishing (L = 3 mm and L = 6 mm) when the fluid pressure is 8 bar. (a) Simulation results of the fluid velocity distribution (section view), (b) simulation results of the turbulence intensity ratio distribution (section view), (c) sectional profile of fluid velocity with the distance of 3mm to the orifice, and (d) sectional profile of turbulence intensity ratio with the distance of 3mm to the orifice

3 Experimental analysis

To further validate the feasibility of FLJP, a series of experiments were conducted to test its material removal characteristic. Figure 4 shows the prototype of the experimental setup for these experiments, which were conducted on a *ZEEKO IRP200* ultra-precision polishing machine. A FLJP nozzle with 3 mm length and 0.5 mm width line orifice was purposely designed for this study as shown in Fig. 4.

The material of the nozzle is 440C stainless steel. When polishing the cylindrical surface, nozzle was adjusted to be perpendicular to the axis of the cylinder through controlling A-axis, B-axis. Moreover, the workpiece was moved to the same height of the line orifice as shown in Fig. 4. During polishing, the workpiece was controlled to feed in Z direction together with rotation along C-axis. The materials of all workpiece used in these experiments are 304 stainless steel. 1000# SiC mixed with water was adopted as the polishing slurry.

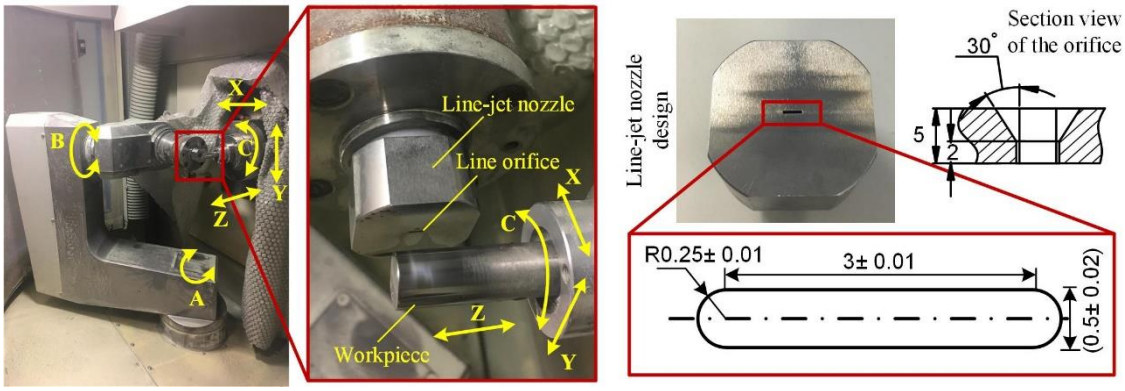

Fig. 4 Snapshot of the experimental prototype for fluid line-jet polishing the roller surface.

3.1 Comparison of tool influence function comparison between fluid line-jet polishing and traditional fluid jet polishing

To analyze the enhancement of the material removal rate of FLJP as compared to FJP, experiment was conducted to generate their tool influence functions (TIFs). The diameter of the orifice in FJP is 0.5 mm. The value of fluid jet size ratio η is 8.64 calculated according to Eq.(1). The TIFs of them were generated under the same polishing conditions as summarized in Table 1. The dwell time of them are all 3min to generate reasonable material removal depth for better TIF measurement.

Table 1 Tool influence function generation conditions

Polishing condition	**value**
Fluid pressure (bar)	6
Stand-off distance (mm)	3
Impinging angle (deg)	90
Slurry concentration (wt.%)	10

The generated TIFs were measured by a Zygo NexView 3D optical profilometer. Figure 5 shows the measured TIFs of FJP and FLJP. Their 3D contours are shown in Fig. 5(a) and 5(b), and corresponding sectional profiles are shown in Fig. 5(c) and 5(d). Similar to the FJP, there also exist non-material removal zone at the center region in FLJP induced by the stagnation zone as shown in Fig. 5(b). Besides, there exist two different kinds of removal region. One is the deeper removal region at the top and bottom part (defined as 'zone 1') of the TIF, the other is the shallower and long removal region at the left and right part (defined as 'zone 2'), which can be obviously observed in Fig. 5(d). The shape of zone 1 is similar to the half TIF of FJP, which is related to the semicircle end shape of the line orifice. While the material removal is quite uniform in zone 2, which attributes to the uniform fluid impinging velocity along the length direction of the line orifice as shown in Fig. 2(a). These characteristics of the TIF depicts that the material removal mechanism of FLJP is similar to FJP, which are all mainly induced by the abrasive cutting or ploughing the target surface in tangential direction. The uniform material removal of zone 2 is beneficial for the implementation of uniform polishing, especially for the components having long and narrow target surface.

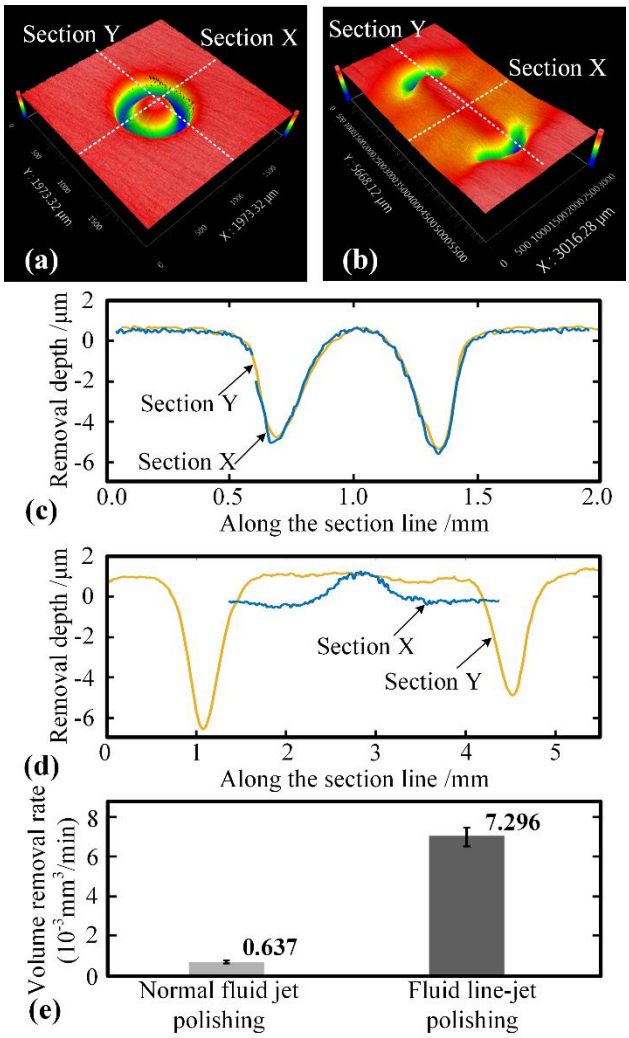

Fig. 5 Tool influence function (TIF) comparison between fluid line-jet polishing (FLJP) and normal fluid jet polishing (FJP). (a) Measured TIF contour of FJP, (b) measured TIF contour of FLJP, (c) sectional TIF profile of FJP along the line shown in (a), (d) sectional TIF profile of FLJP along the line shown in (b), and (e) volume removal rate (*VRR*) comparison between FJP and FLJP.

The material removal rate between FJP and FLJP was compared based on their material volume removal rate (*VRR*), and the *VRR* comparison result has been presented in Fig. 5(e). The average *VRR* of FLJP under the conditions shown in Table 1 is 7.296×10^{-3} mm^3/min, while it is 0.637×10^{-3}

mm^3/min of FJP. The enhancement of the material removal rate is noteworthy through adopting FLJP, which is about 1145% as compared to FJP. Considering that the material removal in FLJP is mainly induced by the material erosion induced by the abrasive impinging, the total volume of material removal V_{total} can be approximately estimated by:

$$V_{total} = \iint_{\Omega} Q_{erosion}(x,y)dxdy \tag{6}$$

where Ω is the size of the erosion region, $Q_{erosion}(x,y)$ is the material erosion volume at the position (x,y), which can be expressed as

$$Q_{erosion}(x,y) = N_p(x,y,w,v_s,...)\cdot\Delta Q_{erosion}(x,y,v_0,\theta_0,d_p,\rho_p,...) \tag{7}$$

where N_p is the abrasive particle spatial distribution, which is determined by the slurry concentration w, slurry velocity v_s, nozzle shape, etc. And $\Delta Q_{erosion}$ is the volume removed by a single particle with initial impinging velocity v_0 and impinging angle θ_0, it is also influenced by the abrasive diameter d_p, abrasive material density ρ_p, and other material properties of the abrasive and target surfaces. The size of the erosion region Ω of FLJP is much larger than FJP, which is the main reason for the enhancement of the material removal rate under the same polishing conditions. The enhancement can be scaled much larger by using longer line-jet orifice with larger η as compared to normal circle orifice.

3.2 Tool influence function under different polishing conditions

A series of experiments were also conducted to investigate the effect of some main factors influencing on the FLJP process, including SOD, fluid pressure and dwell time. The TIFs under different conditions were generated on 304 stainless steel flat surface. Table 2 shows the experimental design. 1000# Silicon carbide (SiC) mixed with water was adopted as the polishing slurry.

Table 2 Experimental design

Polishing condition	Group 1	Group 2	Group 3
Stand-off distance (mm)	1,2,3,4,5	3	3
Fluid pressure (bar)	6	4,5,6,7,8	6
Dwell time (min)	3	3	2,4,6,8,10

The generated TIFs were measured by a Zygo NexView 3D optical profilometer. The sectional profiles in two directions of the measured TIFs have been extracted and compared as shown in Figs. 6(a) to Fig. 6(c). The VRR of them were also determined according to Eq. (5) and presented in Fig. 6(d) so as to quantitatively analyze their effect to the material removal rate. It is interesting to note that the fluid pressure has much more notable effect on the material removal rate than SOD. Higher fluid pressure leads to much larger material removal rate, while the relationship between SOD and the removal rate is insignificant. This phenomenon is similar to FJP [5] since their material removal are all caused by the abrasives impinging the target surface. According to the reported literature [23], the erosion of a single particle $\Delta Q_{erosion}$ during the process can be approximately estimated by the following equation when the erosion process is dominated by the cutting process.

$$\Delta Q_{erosion} = c_1 m_p \rho_p^{c_2} d_p^{c_3} v_0^{c_4} (\cos\theta)^{c_5} (\sin\theta)^{c_6} \tag{8}$$

where $c_1 \sim c_6$ are constant coefficients which are related to the material properties, and m_p is the particle's mass. The particle impinging velocity v_0 becomes higher with increasing fluid pressure which leads to the enhancement of $\Delta Q_{erosion}$. Hence, the increase of the fluid pressure can directly boost the material removal rate. It is also interesting to note that the increased removal depth is almost

proportional to the increase of the dwell time as shown in Fig. 6(c) and Fig. 6(d). It infers that the FLJP has high controllability of material removal during the polishing process.

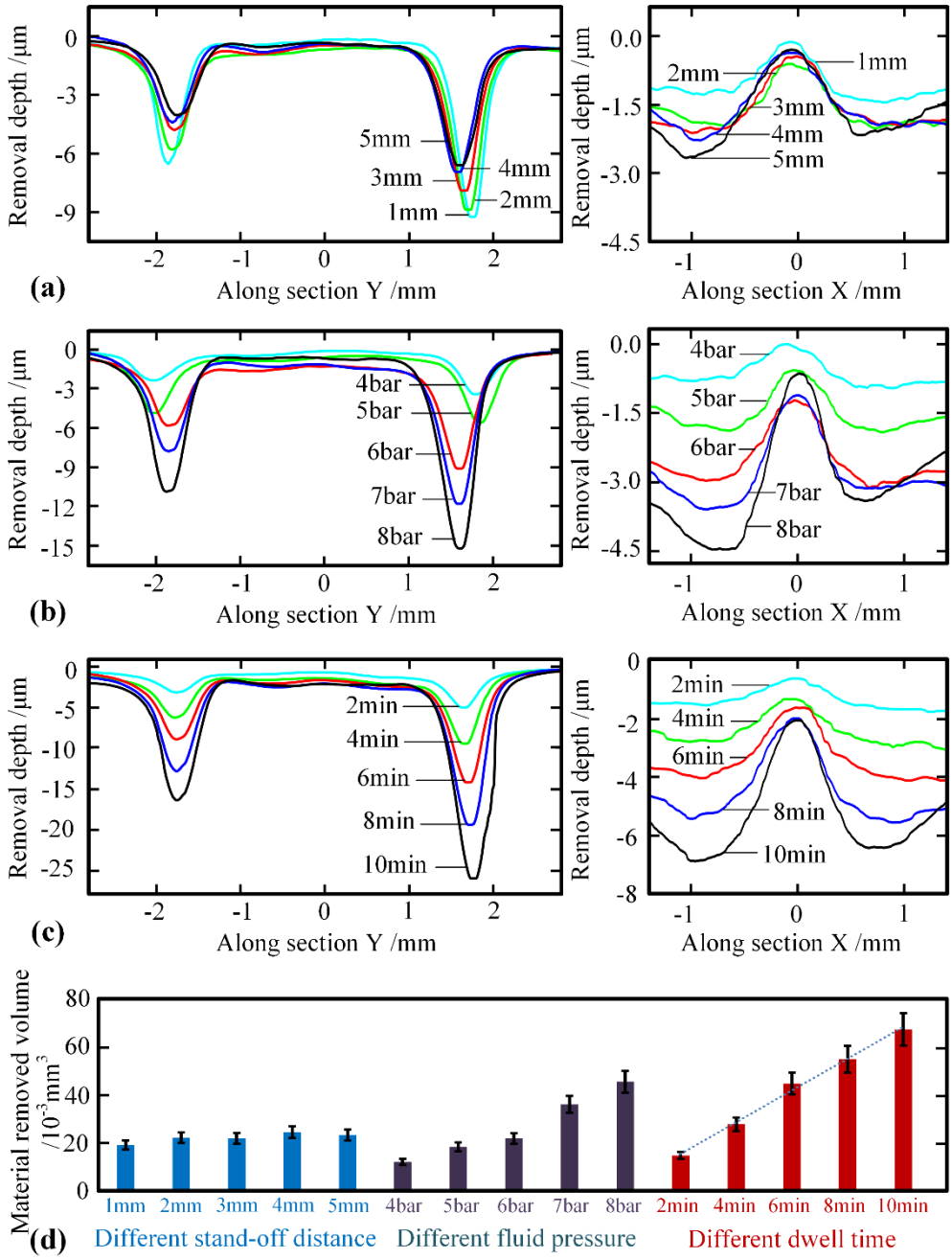

Fig. 6 Tool influence function (TIF) analysis under different polishing conditions. Sectional profiles of TIFs in X and Y direction (a) under different stand-off distance, (b) under different fluid pressure, and (c) under different dwell time. (d) Material removed volume analysis under different polishing conditions.

3.3 Comparison of polishing uniformity between fluid line-jet polishing and linear array multi-jet polishing

In this section, an uniform removal experiment was conducted to realize the technological advantage of the polishing uniformity of FLJP as compared to linear array multi-jet polishing (called 'MJP' for short) [20]. A linear distributed 4-jet nozzle, whose orifice diameter is 0.5 mm with 1 mm orifice interval, was used in the comparison. The experiment was conducted on flat surfaces. Both of them were controlled to move on a line path with the length of 5 mm, and the feed rate was 0.5 mm/min. Other polishing conditions were the same as summarized in Table 1.

Figure 7 shows the measured material removal distribution after uniform polishing along a line. The material removal contour after uniform polishing adopting MJP is shown in Fig. 7(a), and sectional profiles along the lines as shown in Fig. 6(a) have been extracted as depicted in Fig. 7(b). Figure 7(c) demonstrates the measured material removal contour after uniform polishing adopting a line-jet nozzle, and the corresponding sectional profiles are shown in Fig. 7(d). It is interesting to note that the material removal distribution in most of the central part after FLJP as highlighted in a block in Fig. 7(c) and Fig. 7(d) shows much more uniform material removal of FLJP than that for MJP. This is another technological merit for FLJP, which is specifically useful when the target surface is shallower than the length of the line orifice. When the target surface is shallower than the length of the line orifice, the target surface can just be put at the position inside the uniform polishing zone to implement uniform material removal and no need to feed along the axis direction of the RAS, while the feed movement is still needed when using MJP.

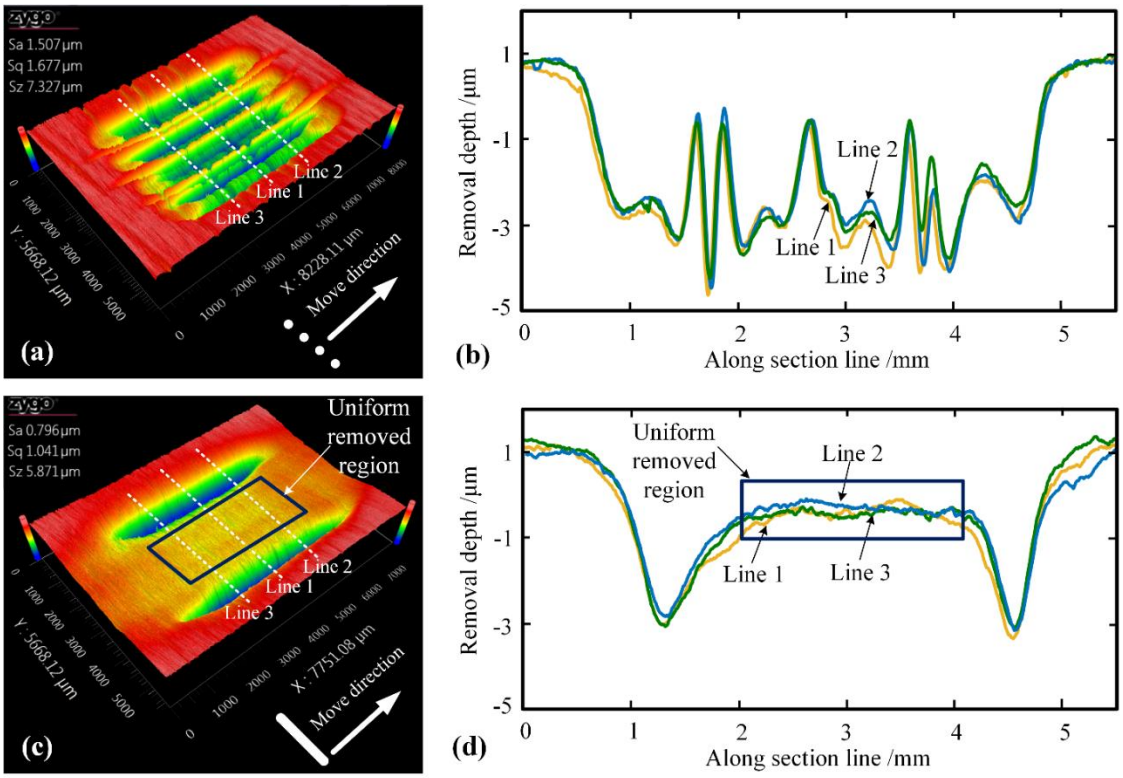

Fig. 7 Material removal distribution comparison between multi-jet polishing (MJP) and fluid line-jet polishing (FLJP). (a) Measured contour of material removal of MJP, (b) sectional profiles of the material removal distribution of MJP, (c) measured contour of material removal of FLJP, and (d) sectional profiles of the material removal distribution of FLJP.

3.4 Polishing experiments on cylindrical surfaces

To further demonstrate the polishing performance of FLJP on cylindrical surfaces, uniform polishing experiments on 3 samples were conducted. Sample 1# and sample 2# were polished by FLJP, while sample 3# was polished by FJP for comparison. The diameter of the cylindrical samples as shown in Fig. 3 is 12.5 mm. When polishing the cylindrical surface, nozzle was adjusted to be perpendicular to the axis of the cylinder through controlling A-axis, B-axis. Moreover, the workpiece was moved to the same height of the line orifice as shown in Fig. 3. During polishing, the workpiece was controlled to feed in Z direction together with the rotation along C-axis. The polishing length on

the samples are all 15 mm. Other polishing conditions have been summarized in Table 3.

Table 3 Experimental conditions of polishing on cylindrical surfaces

Polishing condition	**Sample 1#**	**Sample 2#**	**Sample 3#**
Polishing method	FLJP	FLJP	FJP
Surface preparation	Rough ground	Fine ground	Fine ground
Feed rate (mm/min)	0.5		
C-axis rotation speed (rpm)	5		
Stand-off distance (mm)	3		
Fluid pressure (bar)	6		
Impinging angle (deg)	90		
Slurry concentration (wt.%)	10		

Figure 8 shows the polished surface and the results of surface roughness analysis. Mirror-like surfaces were obtained after FLJP and FJP as shown in Fig. 8(a). Three different points on each sample were measured for analysis. The arithmetic roughness Ra of two ground surfaces were improved from 220.7 nm and 47.3 nm to 42.3 nm and 24.6 nm respectively after one cycle of polishing as shown in Fig. 8(b), which indicates that the FLJP is effective to improve the surface roughness of the cylindrical surfaces. Under the same polishing conditions, the arithmetic roughness Ra of sample 3# after FJP was improved from 38.3 nm to 30.3 nm. It suggests that the surface roughness after FLJP is as well as FJP.

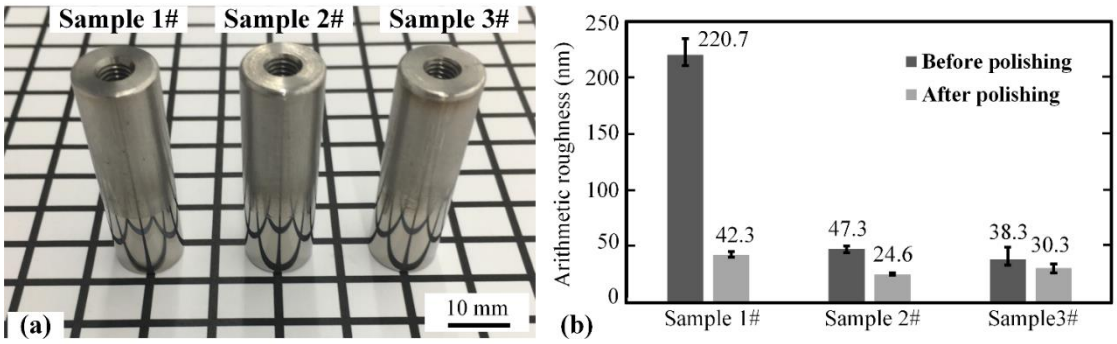

Fig. 8 Polished surface and roughness analysis results. (a) Snapshots of three polished samples, and (b) arithmetic surface roughness of the cylindrical surfaces before and after polishing.

Moreover, the measured surface roughness results from Zygo NexView 3D optical profilometer were also compared as shown in Fig. 9. As for sample 1#, the rough ground marks have relatively high peak-to-valley value, which has not been eliminated after one pass of FLJP as shown in the left-bottom part of Fig. 9. This can also be reflected from the snapshot as shown in Fig. 8(a), in which the snapshot of sample 1# is not as clear as sample 2# and 3#. The fine ground mark of sample 2# and sample 3# was completely removed, only plenty of pits were left induced by the collisions of the abrasives. Scan Electron Microscope (SEM) photos of the polished surfaces were also taken on Hitachi Electron Microscope TM3000 for observation of material removal in micro-scale as shown in Fig. 10, including surfaces magnified by 500× and 5000×. It is interesting to note that the surface character in micro-scale after FLJP is almost the same as the surface after FJP, on which there are many pits attribute to the material removal in ploughing or cutting way by the abrasive.

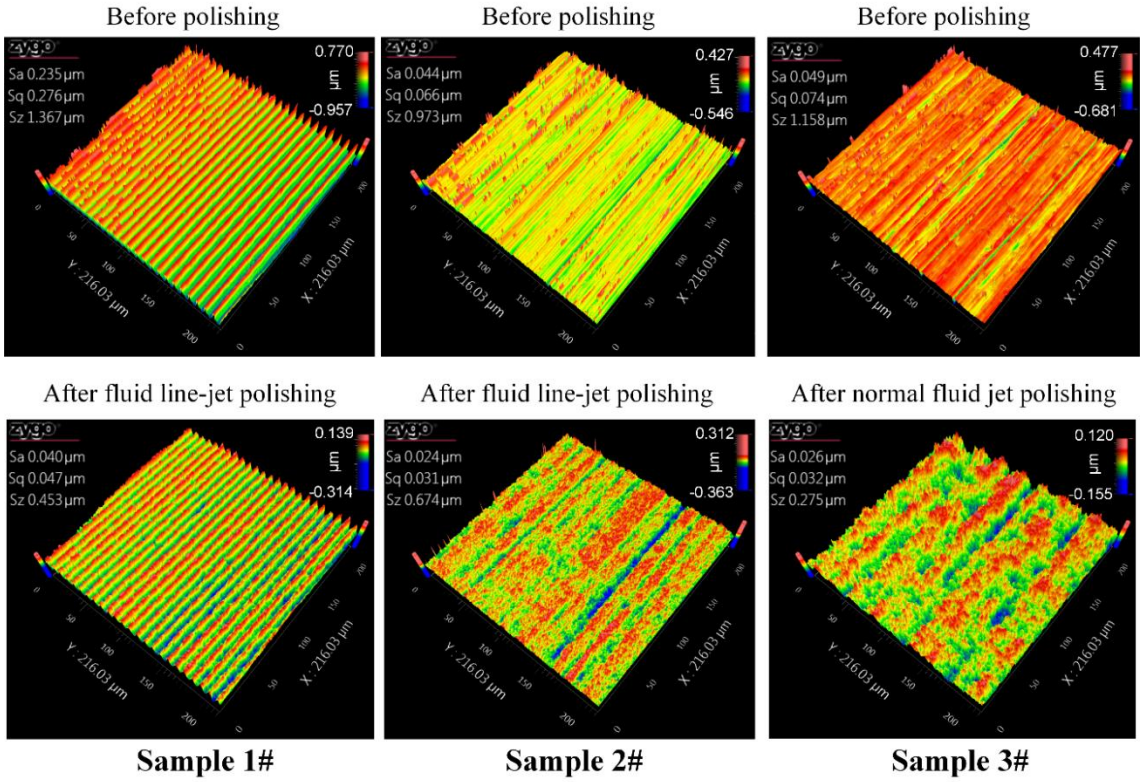

Fig. 9 Comparison of measured surface roughness profiles before and after fluid line-jet polishing and normal fluid jet polishing

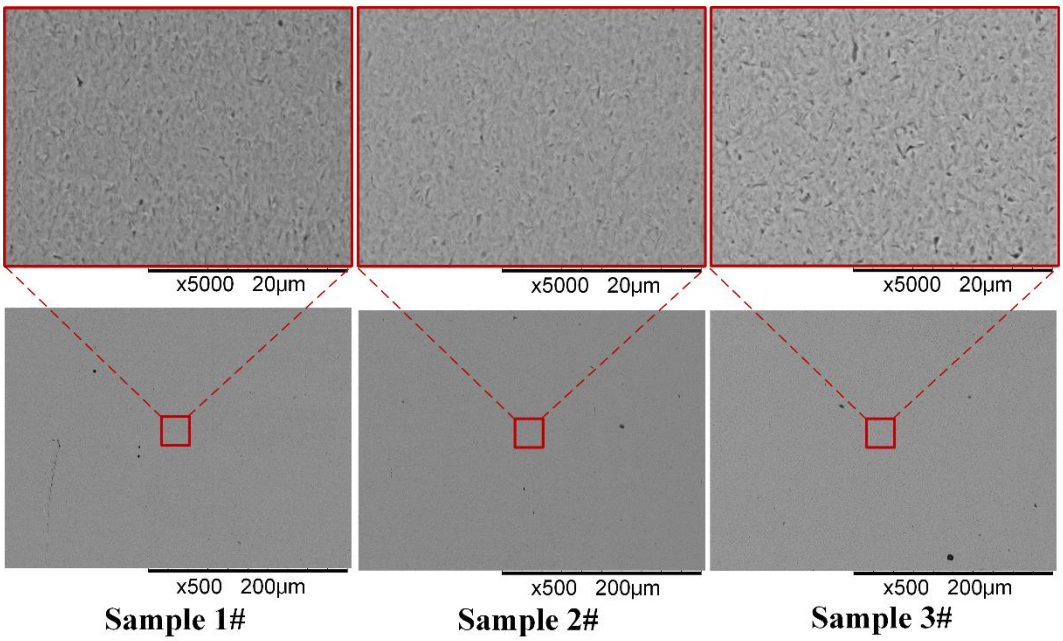

Fig. 10 Comparison of measured SEM results of surfaces after fluid line-jet polishing and normal fluid jet polishing.

4 Potential applications of fluid line-jet polishing

FJP can be used to polish various kinds of freeform surfaces made of most of kinds of materials, including metals, ceramics, glasses, etc. According to the polishing performance analysis above, FLJP performs much better than FJP and MJP when polishing the RAS, due to its high material removal rate and polishing uniformity. RAS have been widely used in bearings, piston rings, and linear slides, etc. Figure 11 shows the application of FLJP when polishing the RAS with narrow target surface. In this case, the width of the target surface is smaller than the length of the line orifice. The workpiece is positioned within the uniform material removal zone as shown in Fig. 7(d), only the rotation of the workpiece is needed during the whole polishing process. It will make the polishing process much more efficient and easy to control. Moreover, the fluid line-jet polishing can also be used for the polishing of RAS with long target surface, in which the length of the target surface is larger than the line orifice. Under this situation, feeding movement along the axis direction is needed for the nozzle to scan the whole target surface. In addition, the FLJP can also be adopted for the polishing of other freeform surfaces as shown in Fig. 13.

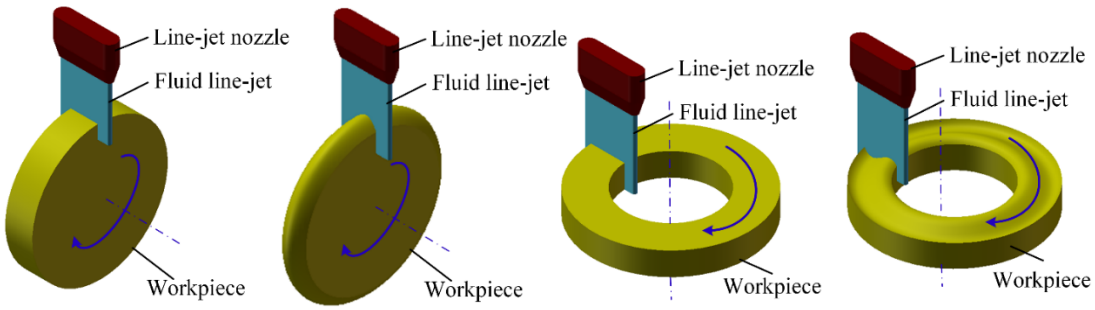

Fig. 11 Applications of fluid line-jet polishing on axisymmetric surfaces with narrow target surfaces

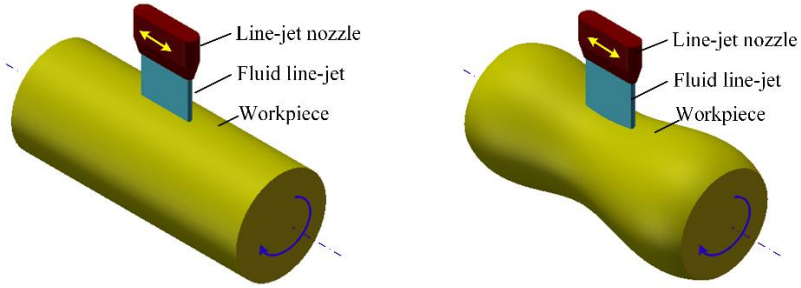

Fig. 12 Application of fluid line-jet polishing on axisymmetric surfaces with long target surfaces

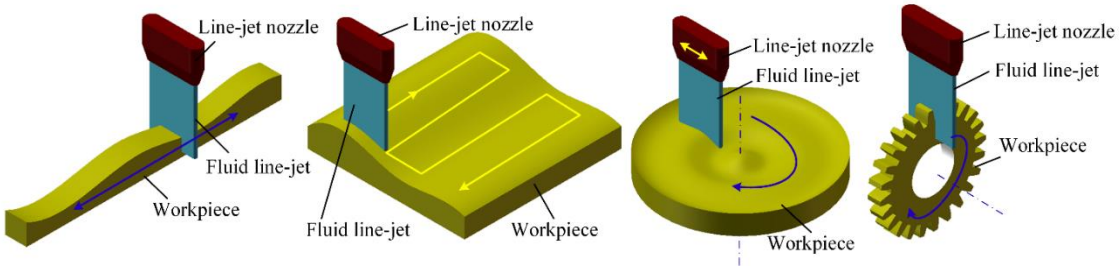

Fig. 13 Application of fluid line-jet polishing for other kinds of freeform surfaces

5 Conclusions

In this paper, a novel FLJP polishing process, which innovatively adopts a line-shape orifice to generate the fluid jet, is presented, which attempts to enhance the polishing efficiency of FJP without degrading the surface integrity, and implement more uniform material removal than MJP on RAS. The following conclusions can be drawn based on the theoretical analysis and experimental results:

(1) The material removal rate was largely increased through adopting the FLJP process as compared to traditional FJP. The enhancement of the material removal rate reached 1145% under the same polishing process parameters, when the length and width of the line-orifice are 3 mm and 0.5 mm respectively, while the diameter of the circle orifice is 0.5 mm. Moreover, the enhancement of the material removal rate is scalable when the ratio is increased between the length and the width of the line orifice.

(2) Different with FJP, the TIF of FLJP has a uniform removal region along the length direction of the

line orifice, which is very helpful for uniform polishing of RAS, especially for the ones having narrow target surface.

(3) FLJP process is effective to improve the surface quality, and the polished surface integrity is as well as the surface polished by traditional FJP under the same polishing conditions.

(4) The relationship between the polishing factors and the material removal rate in FLJP is similar to FJP, due to the same material removal mode, which makes it possess good material removal controllability.

Acknowledgements

The work described in this paper was mainly supported by a grant from the Research Grants Council of the Government of the Hong Kong Special Administrative Region, China (Project No. 15200119). The authors would also like to express their sincerely thanks to the financial support from the Guangdong Natural Science Foundation Programme 2019-2020 (Project No.: 2019A1515012015).

References

[1] Zhang X, Huang R, Liu K, Kumar AS, Shan X. Rotating-tool diamond turning of Fresnel lenses on a roller mold for manufacturing of functional optical film. Precis Eng 2018; 51:445-57.

[2] Khalilpourazary S, Salehi J. How alumina nanoparticles impact surface characteristics of Al7175 in roller burnishing process. Journal of Manufacturing Processes 2019; 39:1-1.

[3] Guo J, Au KH, Sun CN, Goh MH, Kum CW, Liu K, Wei J, Suzuki H, Kang R. Novel rotating-vibrating magnetic abrasive polishing method for double-layered internal surface finishing. Journal of Materials Processing Technology. 2019; 264:422-37.

[4] Fähnle OW, Van BH, Frankena HJ. Fluid jet polishing of optical surfaces. Appl Opt 1998; 37: 6771–6773.

[5] Booij SM. Fluid jet polishing: possibilities and limitations of a new fabrication technique. PhD Thesis 2003; Technical University of Delft.

[6] Beaucamp A, Namba Y, Freeman R. Dynamic multiphase modeling and optimization of fluid jet polishing process. Ann CIRP 2012; 61:315–318.

[7] Shiou FJ, Asmare A. Parameters optimization on surface roughness improvement of Zerodur optical glass using an innovative rotary abrasive fluid multi-jet polishing process. Precis Eng. 2015; 42:93-100.

[8] Tsai FC, Yan BH, Kuan CY, Huang FY. A Taguchi and experimental investigation into the optimal processing conditions for the abrasive jet polishing of SKD61 mold steel. Int J Mach Tools Manuf 2008; 48:932–945.

[9] Beaucamp A, Namba Y. Super-smooth finishing of diamond turned hard X-ray molding dies by combined fluid jet and bonnet polishing. Ann CIRP 2013; 62:315–318.

[10] Billingham J, Miron CB, Axinte DA, Kong MC. Mathematical modelling of abrasive waterjet footprints for arbitrarily moving jets: part II—overlapped single and multiple straight paths. Int J Mach Tools Manuf 2013; 68:30-39.

[11] Nouhi A, Spelt JK, Papini M. Abrasive jet turning of glass and PMMA rods and the micro-machining of helical channels. Precis Eng 2018; 53:151-162.

[12] Nouraei H, Kowsari K, Papini M, Spelt JK. Operating parameters to minimize feature size in abrasive slurry jet micro-machining. Precis eng 2016; 44:109-23.

[13] Beaucamp A, Katsuura T, Kawara Z. A novel ultrasonic cavitation assisted fluid jet polishing system. Ann CIRP 2017; 66:301-304.

[14] Wang CJ, Cheung CF, Ho LT, Liu MY, Lee WB. A novel multi-jet polishing process and tool for high-efficiency polishing. Int J Mach Tools Manuf 2017; 115:60-73.

[15] Ho LT. Theoretical and Experimental Investigation of 3D-Structured Surface Generation by Computer Controlled

Ultra-precision Polishing. PhD thesis 2015, The Hong Kong PolyTechnic University.

[16] Messelink WACM, Waeger R, Wons T, Meeder M, Heiniger KC, Faehnle OW. Prepolishing and finishing of optical surfaces using fluid jet polishing. Proc SPIE 2005; 5869:586908-6.

[17] Yu Z, Kuo C, Chen C, Hsu W, Tsai P. Study of air-driving fluid jet polishing. Proc SPIE 2011; 8126:81261–6.

[18] Wang CJ, Cheung CF, Liu MY, Lee WB. Fluid jet-array parallel machining of optical microstructure array surfaces Opt Express 2017; 25:22710-22725.

[19] Cheung CF, Wang CJ, Ho LT, Chen JB. Curvature-adaptive multi-jet polishing of freeform surfaces. Ann CIRP 2018; 67:357-360.

[20] Cheung CF, Wang CJ, Cao ZC, Ho LT, Liu MY. Development of a multi-jet polishing process for inner surface finishing. Precis Eng 2017; 52:112-121.

[21] Wang CJ, Cheung CF, Liu MY. Numerical modeling and experimentation of three dimensional material removal characteristics in fluid jet polishing. Int J Mech Sci 2017; 133:568-577.

[22] ANSYS, Inc (2016), ANSYS Fluent User's Guide, Release 172.

[23] Huang C, Chiovelli S, Minev P, Luo J, Nandakumar K. A comprehensive phenomenological model for erosion of materials in jet flow. Powder Technol 2008; 187:273-279.